Low Power, Compact Integrated Photonic Sampler Based on a Silicon Ring Modulator

Mohamed I. Hosni, Karanveer Singh, Sourav Dev, Arezoo Zarif, Stefan Preussler, Ayman M. Mokhtar, Kambiz Jamshidi, and Thomas Schneider

***Abstract*—Sampling is the primary functional step of an analogue to digital conversion, required for sensing, measurement, signal processing, metrology, and various data communication applications. Here we present, for the first time, to the best of our knowledge, the optical sampling of different microwave signals with sinc-pulse sequences with a very compact integrated silicon photonics ring modulator. By a simple time interleaving with three branches, the employed ring modulator enables ultra-compact photonic integrated analog to digital converters with a sampling rate of three times the RF bandwidth of itself and of the used photodetector and electronic devices. Therefore, its analogue bandwidth is 50% higher than the RF bandwidth of the incorporated electronics and photonics. Thus, the method might enable high-bandwidth analogue to digital converters with ultra-compact footprint and lower power consumption for future communication systems, sensors, and measurement devices.**

***Index Terms*—Optical sampling, ring modulator, silicon photonics, sinc pulse sequences.**

I. Introduction

SAMPLING can be defined in the time domain as the conversion of a continuous signal amplitude into equidistant, discrete time-values. These discrete amplitude-values can be assigned to the closest digital bit-combination, achieving analogue to digital conversion (ADC). To avoid aliasing, the sampling rate should be at least twice the bandwidth of the baseband signal. The performance of an ADC can be characterized by its analogue bandwidth, power consumption, accuracy, and size [1], [2].

For electronic ADCs, sample and hold circuits can be used for sampling. However, the analogue bandwidth of electronic ADCs is a severe bottleneck for high-bandwidth communication systems [3]. Optical sampling methods might be a promising alternative due to possibly higher operational bandwidths at lower power consumption and inherent immunity to electromagnetic interference. One possibility to achieve an ideal sampling is the multiplication of the signal to be sampled with a Dirac Delta Sequence. Such a Dirac Delta sequence can be approximated by the pulse sequences generated by a mode-locked laser (MLL), for instance [4], [5]. Such sampling can show very low jitter and phase noise values [5], [6], but for the multiplication with the signal to be sampled, a nonlinear device is required, which might result in errors and poses a challenge for integration [7].

Since, according to the sampling theorem, every bandwidth-limited signal can be seen as the superposition of time-shifted sinc pulses, weighted with the sampling points and since these pulses are orthogonal, another possibility of ideal sampling is the multiplication of the signal with sinc pulses [8]–[11]. Compared to Dirac Delta sequences, the sampling signal has a limited spectrum, i.e., the sinc pulses just need a minimum bandwidth of twice the bandwidth of the signal to be sampled. This has the special advantage that the sampling pulses can be directly adapted to the signal to be sampled. But, sinc pulses are unlimited in time. However, they can very closely be approximated by sinc pulse sequences, which correspond to a rectangular, phase-locked frequency comb in the frequency domain [12]–[14]. Such combs can be generated with a pulse source and pulse shaping filters [15] or by using intensity modulators, e.g., Mach-Zehnder modulators (MZM), driven with sinusoidal radio frequencies (RF) [12]–[14].

Especially the sinc pulse sequence sampling based on intensity modulators has several advantages. The multiplication of the signal to be sampled with the sinc pulse sequence, is the convolution of the signal spectrum with the rectangular frequency comb [7]–[11]. This convolution can directly be fulfilled in the same modulator which generates the sinc pulse sequences. Thus, if an intensity modulator is used, this single modulator is fulfilling the whole sampling process. It generates the pulse sequences and multiplies them at the same time with the signal to be sampled. Additionally, since MZMs are standard devices of integrated photonics, such sampling is quite simple to integrate. Recently, it has been shown that integrated MZMs can offer excellent performance for sinc pulse sequence generation [16], [17] and sampling [7].

However, integrated MZMs require quite a large chip space and power consumption. The MZM used in [7], for instance,

Manuscript received 23 June 2022; revised 28 July 2022; accepted 3 August 2022. Date of publication 8 August 2022; date of current version 22 August 2022. This work was supported in part by the Deutsche Forschungsgemeinschaft (DFG, German Research Foundation) under Grants 403579441, 424608109, 424608271, 424607946, 424608191, 403154102, and 322402243 and in part by the German Federal Ministry of Education and Research (BMBF, Bundesministeriumfur Bildungund Forschung) under Grant 13N14879. *(Corresponding Author: Mohamed I. Hosni.)*

Mohamed I. Hosni, Karanveer Singh, Stefan Preussler, and Thomas Schneider are with THz Photonics Group, Technische Universitat Braunschweig, 38106 Braunschweig, Germany (e-mail: mohammed.elsayed@ihf.tu-bs.de; karanveer.singh@ihf.tu-bs.de; stefan.preussler@ihf.tu-bs.de; thomas.schneider@ihf.tu-bs.de).

Sourav Dev, Arezoo Zarif, and Kambiz Jamshidi are with Integrated Photonic Devices Group, Technische Universitat Dresden, 01062 Dresden, Germany (e-mail: sourav.dev@tu-dresden.de; arezoo.zarif@mailbox.tu-dresden.de; kambiz.jamshidi@tu-dresden.de).

Ayman M. Mokhtar is with Optoelectronics Department, Military Technical College, 387130 Kobry Elkobh, Cairo, Egypt (e-mail: ayman.mokhtar@mtc.edu.eg).

Digital Object Identifier 10.1109/JPHOT.2022.3197300

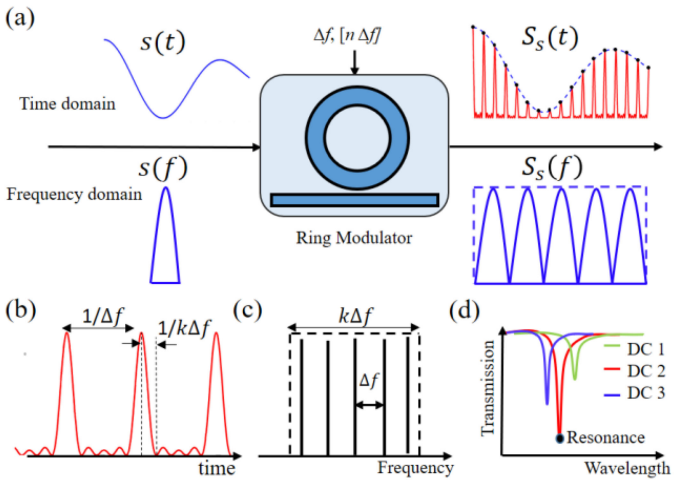

Fig. 1. (a) Concept for optical sampling based on a ring modulator. Please note that the sampler is just the correctly adjusted ring modulator driven with one or several sinusoidal frequencies. The signal to be sampled at the optical input of the modulator and the sampled signal at the output are shown in the time (top) and frequency domain (bottom). (b) Sinc pulse sequence with $1/\Delta f$ repetition rate and $1/(k\Delta f)$ pulse period and corresponding flat frequency comb (c). (d) The transmission spectrum of the ring modulator at different DC biases.

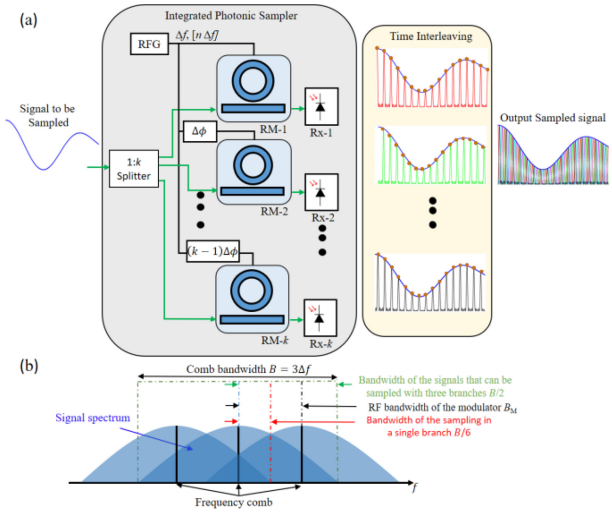

Fig. 2. (a) Concept of a time-interleaved integrated photonic sampler based on silicon ring modulators. The input signal is split into k branches. In each branch, this signal is sampled with a ring modulator driven by n RF frequencies with a proper RF phase shift to adjust the sampling time. The time-interleaved sampling points are taken by the integration with low-bandwidth detectors and can be further processed by low-bandwidth electronics. All photonic and electronic components can be integrated on the same chip. (b) Ring modulator sampling in the frequency domain. The spectrum of the signal to be sampled, having a bandwidth B, is convoluted with a three-line frequency comb with the same bandwidth. The baseband bandwidth of the sampling in a single branch is $B/6$ and with all three branches $B/2 = 1.5 \times B_M$ (modulator bandwidth). RFG: radio frequency generator, RM: ring modulator, and Rx: receiver.

has two phase shifters with a 3.2 mm length and requires an RF power of 14 dBm for each of them. In Ref. [18] the power consumption of the mm-sized MZM was >1 pJ/bit. Ring modulators instead are much more suitable for very compact and low-power integrated systems, because the size of these modulators is in the micrometers scale and the power consumption can be less than 100 fJ/bit [18].

As has been shown, such ring modulators can as well be used for the generation of flat, rectangular frequency combs [19]. However, the sampling of optical signals with compact integrated ring modulators has yet to be shown.

However, the sampling of optical signals with compact integrated ring modulators has yet to be shown. Here we present, for the first time to the best of our knowledge, a compact integrated photonic sampler with low power consumption based on a ring modulator. The silicon ring modulator with a radius of only 20 μm has a sampling rate of 2 GSa/s and only requires 5 dBm RF power. Compared with a 3.2 mm long integrated MZM used for sampling [7], the required RF power is reduced by 12 dB.

In the proof-of concept experiments we were restricted by the very low RF bandwidth of our forward-biased ring modulator. Much higher sampling rates of up to 330 GSa/s, corresponding to analogue bandwidths of 165 GHz, are possible with 110 GHz integrated ring modulators,which have already been shown [20].

II. Principple of Operation

In the time domain, the sampling can be seen as the multiplication of the signal to be sampled with a sinc pulse sequence [7]. This corresponds to the convolution of the spectrum of the signal with a rectangular, flat frequency comb. Here this sampling is carried out by an ultra-compact ring modulator, driven with one or a number of n RF signals with the frequency spacing Δf as shown in Fig. 1(a), (b), and (c). Thus, the corresponding real-time sampling rate would be Δf and for k parallel branches with the same modulator, the real-time sampling rate is $(2n+1)\Delta f = k\Delta f$. The sampling requires the proper adjustment of the bias and driving power [12], [14]. If not a signal spectrum but a single, narrow-band line is used as the input to the ring modulator, it produces a flat, rectangular frequency comb with $k = 2n+1$ lines or a sinc pulse sequence with $k-1$ zero crossings. Since for a high-quality sampling, the adjustment is the same, here we will first discuss the sinc pulse sequence generation by a ring modulator. As shown in Fig. 1(b) and (c), a flat, phase-locked frequency comb with a bandwidth of $B = k\Delta f$, corresponds to a sinc pulse sequence with a duration of $1/B$ (from the maximum to the first zero crossing) [12]–[14]. For such a comb generation with a ring modulator, three steps are required. First, sufficient modulation depth at proper DC bias is needed to avoid higher-order sidebands. The modulation depth of the ring modulator changes according to the applied DC bias, as shown in Fig. 1(d). Secondly, the wavelength of the laser diode (LD), or the optical ring radius, should be adjusted to be at or very near to the resonance wavelength of the ring modulator to get a symmetric frequency comb. Lastly, the RF power must be adjusted for getting a flat comb. Because the resonance of the modulator shifts with the RF power [21], a low RF power is required to minimize this shift. Thus, besides the very small size, the ring modulator consumes also low power [18].

For the sampling the CW input has to be replaced by the signal to be sampled, i.e., the signal will be injected into the optical input of the ring, while one or a number of n equispaced RF frequencies are applied to the electrical input, as shown in Fig. 1(a). This signal is sampled based on the convolution of the spectrum of the signal to be sampled with an $k = (2n + 1)$-line

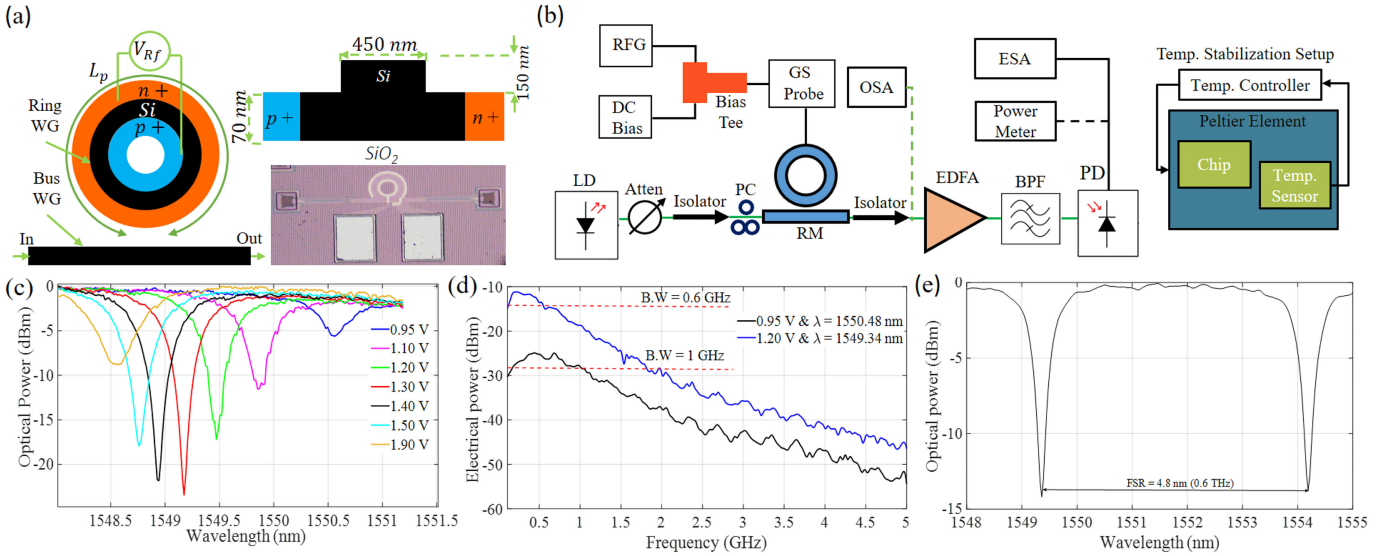

Fig. 3. (a) Schematic of the used ring modulator with PIN junction structure and top view. Experimental setup with temperature stabilization (b). The measured intensity transfer function can be seen in (c), the S21 EO response in (d) and the measured FSR is presented in (e). LD: laser diode, Atten : attenuator, RM: ring modulator, RFG: radio frequency generator, PC: polarizer controller, OSA: optical spectrum analyser, EDFA: erbium doped Fiber amplifier, BPF: bandpass filter, PD: photodiode and ESA: electrical spectrum analyzer.

rectangular, flat frequency comb. The result are k copies of the signal spectrum. In the time domain, this corresponds to the multiplication of the signal to be sampled with a sinc pulse sequence with $k-1$ zero crossings. Thus, the real time sampling rate of a single ring modulator corresponds to the repetition rate of the sequence and is therefore defined by Δf.

To sample the whole signal bandwidth in real time with the sampling rate $k\Delta f$, the input signal has to be time-interleaved as shown in Fig. 2(a). The incoming signal is split into k branches. In each branch a silicon ring modulator is driven with one or n RF frequencies of Δf spacing samples the signal with the sampling rate Δf. To exploit the orthogonality of the sinc pulse sequences, the sampling points taken in the other branches have to be in the zero crossings of the sinc pulse sequence. Thus, the $p-$th ($p = 1, 2, k$) branch needs a time delay of $(p-1)/(k\Delta f)$. This time delay can be achieved by adjusting the phase change of the RF signal driving the ring modulator to $\Delta\phi = 2\pi/k$. Thus, for $n = 1$, the number of spectral copies, corresponding to the number of required branches, will be $k = 3$ and the electrical phases in the three branches have to be 0°, 120°, and 240°, respectively. Since the delay can be adjusted in the electrical domain, no pre-defined time shifters are necessary for the time interleaving. Such a time-shifting is usually carried out by delay lines of a given length. If not compensated, these delay lines lead to an amplitude difference between the copies and they are usually only tunable in a limited range. Thus, only signals of a pre-defined bandwidth can be sampled. Here all parameters like bandwidth, delay, sampling rate and so on are completely defined in the electrical domain by the RF signal driving the ring modulators so that an adjustment of the sampling to the signal to be sampled is simple and fast.

The different bandwidths involved in the sampling process can be seen in Fig. 2(b). The signal spectrum of bandwidth $B = 3 \times \Delta f$ is convoluted with a three-line comb of the same bandwidth. Since in the single sampling branch, an under-sampling is conducted, the spectral copies of the input spectrum are overlapping. Please note, that the necessary sampling rate will be achieved by all three branches together [11], [17]. As can be seen, the modulator with a bandwidth B_M can generate sinc pulse sequences, or a three-line comb, with a bandwidth of three times its RF bandwidth $B = 3 \times \Delta f = 3 \times B_M$ which coincides with the inverse of the pulse duration (peak to first zero crossing) [12]. Following the sampling theorem, in all three branches together a signal with the baseband bandwidth $B/2 = 1.5 \times B_M$ can be sampled.

For sampling the whole information of the signal (amplitude and phase), coherent detectors are necessary [7], [8]. The detection and further processing of the signals with an optical bandwidth B can be carried out with detectors and electrical signal processing with a bandwidth of only $B/(2k)$ [11]. Several low-bandwidth devices are much easier to integrate than a single high-bandwidth one. Therefore, the method enables the detection, reception, and measurement of high-bandwidth signals with very compact, low-bandwidth integrated electronics and photonics.

III. Device Characterization

The structure of the forward-biased ring modulator used for the experiment is shown in Fig. 3(a). It consists of a bus waveguide (WG) and a ring WG. The ring WG has 20 μm radius with a PIN junction working in a forward bias configuration. This junction has 450 nm width, 220 nm height, and 70 nm slab thickness. The length of the junction L_p is equal to 40π μm. The separation between the bus WG and the ring WG is 200 nm. Also, the gap spacing between the electrical pads for driving the optical ring modulator is 100 μm. The integrated chip was fabricated at the Interuniversity Microelectronics Centre (imec).

The electro-optical (EO) modulation in the ring modulator is achieved when an RF signal with proper DC bias is applied. By applying the voltage on the forward-biased junction, carriers will be injected into the WG. Therefore, the concentration of

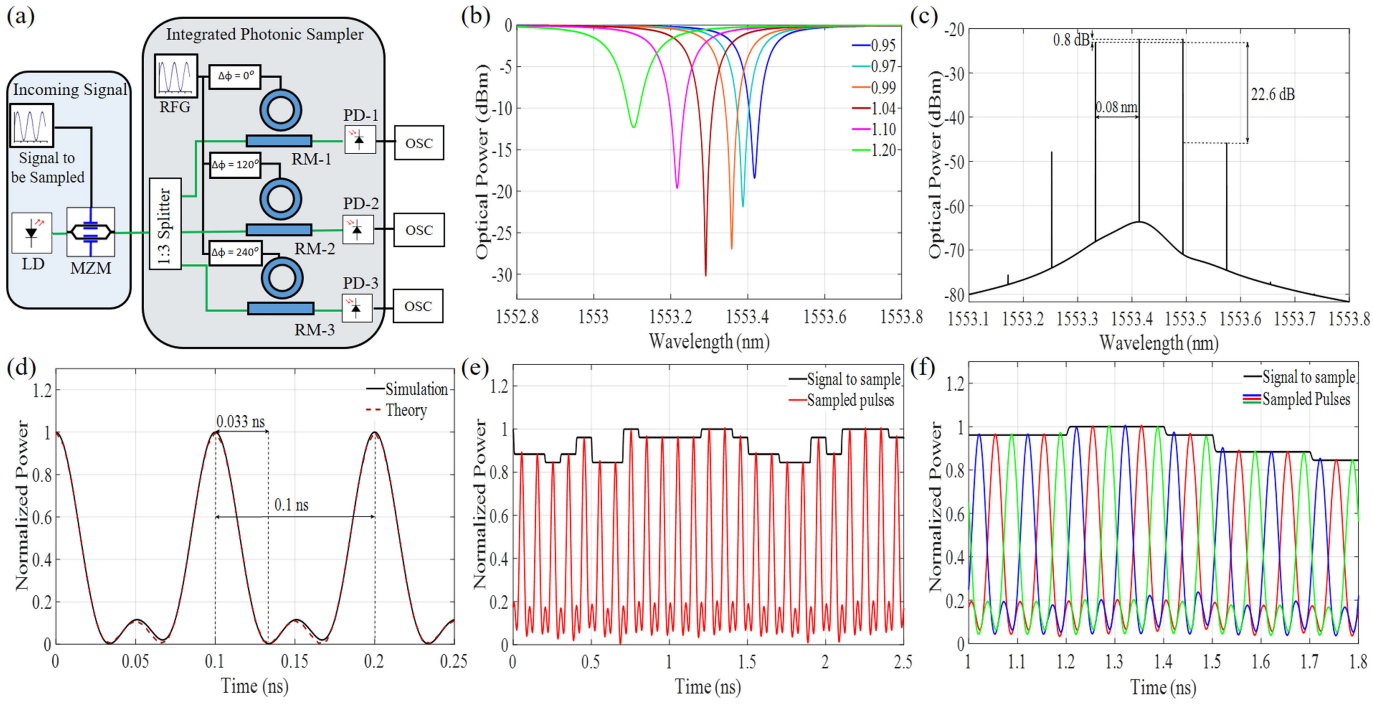

Fig. 4. (a) Simulation setup for the integrated photonic sampler based on a ring modulator with a simulated intensity transfer function (b). (c) The three-lines, flat frequency comb with 0.08 nm (10 GHz) line spacing and comb bandwidth of 30 GHz. The corresponding sinc pulse sequence in the time domain with 0.1 ns repetition rate is shown in (d), (e) presents the sampling of a PAM-4 signal with this setup from a single branch and (f) shows the sampling by three branches. LD: laser diode, MZM: Mach-Zehnder modulator, RFG: radio frequency generator, RM: ring modulator, PD: photodiode and OSC: oscilloscope.

free electrons and holes will be changed and hence, the refractive index and accordingly loss coefficient will be changed [22]–[24].

For device characterization, the experimental setup in Fig. 3(b) was used. This setup contains a temperature stabilization system based on a Peltier element to avoid any shift of the resonance point due to heat dissipation. The temperature of the chip was maintained at 20 °C for all experiments.

For the intensity transfer function measurement, a 1550 nm LD was swept in a range of 16 pm at various DC biases. To avoid any nonlinear effects of the device, the injected optical power into the chip was 0 dBm [25]. The DC bias was applied by a bias tee and ground-source (GS) probe. An optical power meter (Agilent 81638) was used to measure the response of the chip as shown in Fig. 3(b). The measured intensity transfer function in Fig. 3(c) shows a maximum modulation depth of 24 dB for a DC bias of 1.3 V.

The 3 dB electrical bandwidth was measured from the S21 EO response of the ring modulator, as shown in Fig. 3(d). It was measured as 0.6 GHz at 1.2 V DC bias and 1 GHz at 0.95 V. Please note that PIN modulators have a lower bandwidth than PN modulators, because of the limited minority carrier diffusion time inside the PIN junction [18].

The measured FSR was 0.6 THz at 1.2 V as shown in Fig. 3(e). Please note that there is a small shift in the resonance point in Fig. 3(e) compared to Fig. 3(c). Also, the modulation depth in Fig. 3(e) is lower than in Fig. 3(c). This is because we measured the FSR directly from the optical spectrum analyzer (OSA) (Yokogawa AQ6370C) by using a broadband light source, which has a lower resolution compared to the wavelength sweep and power meter as used for Fig. 3(c).

The total optical loss of the integrated ring modulator setup was 12.5 dB including two grating coupler losses with 5 dB each.

IV. Simulation and Experimental Results

First, the ring modulator and sampling of different microwave signals were simulated with the Lumerical software package, afterwards, the experiments were carried out, as presented in this section.

A. Simulation Results

For the simulation, the system in Fig. 4(a) was assumed. The incoming signal to be sampled was split into $k = 3$ branches. In each branch, there is a forward-biased ring modulator. The orthogonality of sampling was achieved by adjusting the phase of the single 10 GHz RF signal driving the ring modulators to 0°, 120°, and 240°. The bandwidth of the simulated modulator was 10 GHz and the modulation depth at 0.95 V is 18 dB as shown in Fig. 4(b). The bandwidth of the simulated modulator was 10 GHz and the modulation depth at 0.95 V is 18 dB as shown in Fig. 4(b). The simulated bandwidth is higher than that of the measured bandwidth of the fabricated device. However, this just results in a higher sampling rate. Please note that the simulations were done at the same modulation depth as that of the experimental work but at a different DC bias. The intensity transfer function of the simulation is different from that in the experiment because of insufficiencies in the fabrication process. At 1.2 V DC bias, a modulation depth of around −12 dB was obtained, and working at this low modulation depth will increase

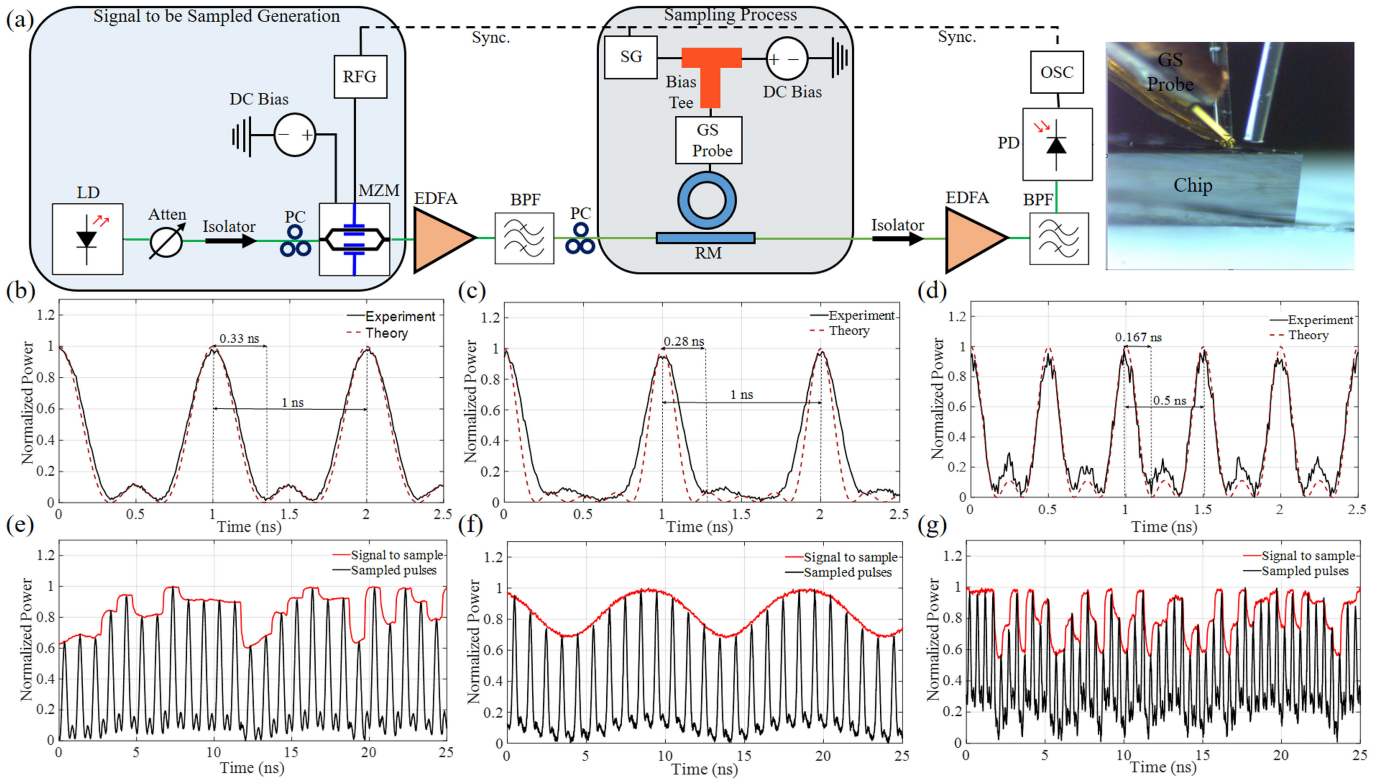

Fig. 5. Experimental setup of the proposed system and a side view of the photonic sampler, the signal to be sampled was generated by using an MZM and was multiplied by the sinc pulse sequence in a ring modulator (a). Sinc pulse sequences were generated by a 1 GHz (b), a 1 GHz and 2 GHz (c) and a single 2 GHz RF signal (d). Sampling of a 1 GBd PAM-4 signal (e), an analog signal of frequency 100 MHz (f) and a 2 GBd PAM-4 signal (g). LD: laser diode, Atten : attenuator, MZM: Mach-Zehender modulator, RM: ring modulator, RFG: radio frequency, PC: polarizer controller, EDFA: erbium doped Fiber amplifier, BPF: bandpass filter, PD: photodiode and OSC: oscilloscope.

the effect of the higher order sidebands and hence the quality of the sampling [26], [27].

For sampling, the LD with an input power of 0 dBm was adjusted to the resonance point of the ring modulator (1553.43 nm). When the optical input is a single line and the ring modulator is driven with only one single RF frequency, the output of the ring modulator is a flat, three-line comb, which can be seen in Fig. 4(c) for a 10 GHz RF signal. The corresponding sinc pulse sequence with 0.1 ns repetition rate and 0.033 ns pulse period is depicted in Fig. 4(d). As can be seen, the sequence shows very small distortions, which are a result of the small asymmetry of the frequency comb.

The single input laser line was then replaced by a 10 GBd PAM-4 signal for sampling. As shown in Fig. 4(e), the sampling follows the signal very well. For a high sampling rate, the sampled signals from the three branches are gathered together offline. As shown in Fig. 4(f) almost ideal sampled 10 GBd PAM-4 was achieved and the sampled signal follows the signal to be sampled with very high accuracy.

B. Experimental Results

For an experimental proof of concept, the setup shown in Fig. 5(a) was used. Due to limited lab equipment, we demonstrate only one branch of the proposed system. The signal to be sampled was generated with a $LiNbO_3$ MZM and an arbitrary waveform generator (AWG70001A, left block in Fig. 5(a)). Please note that instead of the MZM another ring modulator can be used and for signals to be sampled already in the optical domain, the whole left block would not be necessary. This signal was injected into the ring modulator for sampling (middle block in Fig. 5(a)). To compensate for the high coupling losses of the proof of concept chip, an amplification together with a filtering of the amplified spontaneous noise was necessary. If the whole system is integrated with the detector into a single chip, for lower coupling losses, this would not be needed.

For driving the ring modulator, a single tone RF frequency, or two equispaced frequencies were used. These frequencies were applied to the ring modulator together with a 1.2 V DC bias. As shown in Fig. 3(c and d), for a wavelength of 1549.47 nm a modulation depth of 17.2 dB with 0.6 GHz bandwidth was obtained. The optical power injected into the chip was 0 dBm. The sampled signal was measured by a photodiode and an electrical sampling oscilloscope (OSC) (Agilent 86100C).

By adjusting the wavelength of the LD to 1549.6 nm and applying a 1 GHz frequency with 3 dBm power to the ring modulator, the sinc pulse sequence with 1 ns repetition rate shown in Fig. 5(b) was generated. As can be seen, it is very close to the ideal one. Please note that the corresponding three lines flat frequency comb cannot be shown here because of the limited resolution of our optical spectrum analyzer. Sampling was achieved by replacing the laser line with a 1 GBd PAM-4 signal, as presented in Fig. 4(e).

To generate a 5-line comb by the ring modulator, two RF frequencies (1 GHz and 2 GHz) with a total power of 9 dBm were used to generate a sinc pulse sequence with 1 ns repetition rate, as shown in Fig. 5(c). Since 2 GHz is already higher than the electrical bandwidth of the ring modulator, the generated sinc pulse sequence shows a higher distortion compared to the three-line case. However, with the same setup the modulator was used to sample a sinusoidal signal with a frequency of 100 MHz (Fig. 5(f)).

In Fig. 5(d), the ring modulator was driven with one single 2 GHz frequency with 5 dBm electrical power to generate a three-line comb and the corresponding sinc pulse sequence. As this is again above the bandwidth of the ring, small distortions can be seen. The same setup was used for the sampling of a 2 GBd PAM-4 signal, as presented in Fig. 5(g).

All experiments were carried out at 1.2 V bias, resulting in only 0.6 GHz bandwidth. A bias of 0.95 V would result in a higher bandwidth of 1 GHz but also in a low modulation depth of 5 dB, since there is a tradeoff between the bandwidth and modulation depth [28]. Working at lower modulation depths would increase the sideband power and affects the flatness of the frequency comb, which would result in lower quality sampling [26], [27].

V. Conclusion

In conclusion, a compact, low-power integrated photonic sampler based on a carrier injection ring modulator with 20 μm radius was simulated and demonstrated experimentally. By a simple time-interleaving in three branches, the ring modulator can sample signals with three times its RF bandwidth. The whole sampling system can receive, analyze and process signals with an optical bandwidth B with photodiodes and electronics with a bandwidth of only $B/(2k)$. Since only standard equipment is used, no delay lines are required and high-bandwidth signals can be processed with low bandwidth electronics and photonics, the integration of the whole sampling system is straightforward. Such a sampler can be used as a low footprint ADC or agnostic transceiver system [7], [29]. In the proof of concept experiments, the bandwidth of the ring modulator was restricted to only 0.6 GHz. However, ring modulators with bandwidths of 110 GHz have been shown [20], suggesting ultra-compact ADC with 330 GSa/s sampling rate and analogue bandwidths of 165 GHz.

Acknowledgment

The authors would like to thank Meysam Namdari from TU-Dresden for preparing the layout of the Chip, Youns Mandalawi, Janosch Meier, Evans Baidoo, and Arijit Misra from TU-Braunschweig for the constructive discussions.

References

[1] R. H. Walden, "Analog-to-digital converter survey and analysis," *IEEE J. Sel. Areas Commun.*, vol. 17, no. 4, pp. 539–550, Apr. 1999.

[2] R. van de Plassche, *CMOS Integrated Analog-to-Digital and Digital-to-Analog Converters*. New York, NY, USA: Springer-Verlag, 2013.

[3] M. Nagatani et al., "110-GHz-bandwidth InP-HBT AMUX/ADEMUX circuits for beyond-1-Tb/s/ch digital coherent optical transceivers," in *Proc. IEEE Custom Integr. Circuits Conf.*, 2022, pp. 1–8.

[4] A. Khilo et al., "Photonic ADC: Overcoming the bottleneck of electronic jitter," *Opt. Exp.*, vol. 20, no. 4, pp. 4454–4469, Feb. 2012.

[5] A. H. Nejadmalayeri et al., "Attosecond photonics for optical communications," in *Proc. Opt. Fiber Commun. Conf. Expo. /Nat. Fiber Opt. Eng. Conf.*, 2012, pp. 1–3.

[6] R. Salem et al., "High-speed optical sampling using a silicon-chip temporal magnifier," *Opt. Exp.*, vol. 17, no. 6, pp. 4324–4329, Mar. 2009.

[7] A. Misra et al., "Integrated source-free all optical sampling with a sampling rate of up to three times the RF bandwidth of silicon photonic MZM," *Opt. Exp.*, vol. 27, no. 21, pp. 29972–29984, Sep. 2019.

[8] S. Preußler et al., "Frequency-time coherence for all-optical sampling without optical pulse source," *Sci. Rep.*, vol. 6, no. 1, pp. 1–10, Sep. 2016.

[9] J. Meier, A. Misra, S. Preußler, and T. Schneider, "Orthogonal full-field optical sampling," *IEEE Photon. J.*, vol. 11, no. 2, Apr. 2019, Art. no. 7800609.

[10] J. Meier et al., "Optical convolution with a rectangular frequency comb for almost ideal sampling," in *Proc. Next-Gener. Opt. Commun.: Compon. Sub-Syst. Syst. VIII*, 2019, vol. 10947, pp. 108–115.

[11] J. Meier, K. Singh, A. Misra, S. Preußler, J. C. Scheytt, and T. Schneider, "High-bandwidth arbitrary signal detection using low-speed electronics," *IEEE Photon. J.*, vol. 14, no. 2, Apr. 2022, Art. no. 5515207.

[12] M. A. Soto et al., "Optical sinc-shaped Nyquist pulses of exceptional quality," *Nature Commun.*, vol. 4, no. 1, pp. 1–11, Dec. 2013.

[13] S. Preußler, N. Wenzel, and T. Schneider, "Flexible Nyquist pulse sequence generation with variable bandwidth and repetition rate," *IEEE Photon. J.*, vol. 6, no. 4, Aug. 2014, Art. no. 7901608.

[14] M. A. Soto et al., "Generation of Nyquist sinc pulses using intensity modulators," in *Proc. CLEO: Sci. Innov.*, 2013, pp. 1–2.

[15] M. Nakazawa et al., "Ultrahigh-speed orthogonal TDM transmission with an optical Nyquist pulse train," *Opt. Exp.*, vol. 20, no. 2, pp. 1129–1140, Jan. 2012.

[16] S. Liu et al., "Optical frequency comb and Nyquist pulse generation with integrated silicon modulators," *IEEE J. Sel. Topics Quantum Electron.*, vol. 26, no. 2, Mar./Apr. 2020, Art. no. 8300208.

[17] A. Misra et al., "Reconfigurable and real-time high-bandwidth Nyquist signal detection with low-bandwidth in silicon photonics," *Opt. Exp.*, vol. 30, no. 16, pp. 13776–13789, Apr. 2022.

[18] G. Li et al., "Ring resonator modulators in silicon for interchip photonic links," *IEEE J. Sel. Topics Quantum Electron.*, vol. 19, no. 6, Nov./Dec. 2013, Art. no. 3401819.

[19] I. Demirtzioglou et al., "Frequency comb generation in a silicon ring resonator modulator," *Opt. Exp.*, vol. 26, no. 2, pp. 790–796, Jan. 2018.

[20] Y. Zhang et al., "240 Gb/s optical transmission based on an ultrafast silicon microring modulator," *Photon. Res.*, vol. 10, no. 4, pp. 1127–1133, Mar. 2022.

[21] K. P. Nagarjun et al., "Microwave power induced resonance shifting of silicon ring modulators for continuously tunable, bandwidth scaled frequency combs," *Opt. Exp.*, vol. 28, no. 9, pp. 13032–11304, Apr. 2020.

[22] O. Dubray et al., "Electro-optical ring modulator: An ultracompact model advances for the comparison and optimization of p-n, p-i-n, and capacitive junction," *IEEE J. Sel. Topics Quantum Electron.*, vol. 22, no. 6, Nov./Dec. 2016, Art. no. 3300110.

[23] B. B. Bhowmik et al., "Proposal for an optical multicarrier generator based on single silicon micro-ring modulator," *Opt. Commun.*, vol. 349, pp. 132–137, Aug. 2015.

[24] S. Dev et al., "Compact and energy-efficient forward-biased PN silicon Mach-Zehnder modulator," *IEEE Photon. J.*, vol. 14, no. 2, Apr. 2022, Art. no. 6616507.

[25] D. Gray et al., "Thermo-optic multistability and relaxation in silicon microring resonators with lateral diodes," *Phys. Rev. Appl.*, vol. 14, no. 2, Aug. 2020, Art. no. 024073.

[26] S. De, A. Misra, R. Das, T. Kleine-Ostmann, and T. Schneider, "Analysis of non-idealities in the generation of reconfigurable sinc-shaped optical Nyquist pulses," *IEEE Access*, vol. 9, pp. 76286–76295, 2021.

[27] S. De et al., "Roll-off factor analysis of optical Nyquist pulses generated by an on-chip Mach-Zehnder modulator," *IEEE Photon. Technol. Lett.*, vol. 33, no. 21, pp. 1189–1192, Nov. 2021.

[28] H. Yu et al., "Trade-off between optical modulation amplitude and modulation bandwidth of silicon micro-ring modulators," *Opt. Exp.*, vol. 22, no. 12, pp. 15178–15189, Jun. 2014.

[29] A. Misra et al., "Agnostic sampling transceiver," *Opt. Exp.*, vol. 29, no. 10, pp. 14828–14840, Apr. 2021.